

To appear in ApJ

Quasars Clustering at $z \approx 3$ on Scales $\lesssim 10h^{-1}$ MpcL. Infante¹*Departamento de Astronomía y Astrofísica, P. Universidad Católica de Chile, Casilla 306, Santiago 22, Chile*

linfante@astro.puc.cl

J. Varela

Instituto de Matemáticas y Física Fundamental, Consejo Superior de Investigaciones Científicas, C/ Serrano 113 B, 28006 Madrid, Spain

M. Moles

Instituto de Astrofísica de Andalucía, Consejo Superior de Investigaciones Científicas, C/ Camino Bajo de Huétor 24, 18080 Granada, Spain

G. Hertling and A. García

Departamento de Astronomía y Astrofísica, P. Universidad Católica de Chile, Casilla 306, Santiago 22, Chile

and

F. Menanteau

*Department of Physics and Astronomy, Johns Hopkins University***ABSTRACT**

We test the hypothesis whether high redshift QSOs would preferentially appear in small groups or pairs, and if they are associated with massive, young clusters. We carried out a photometric search for Ly α emitters on scales $\lesssim 10h^{-1}$ Mpc, in the fields of a sample of 47 $z \approx 3$ known QSOs. Wide and narrow band filter color-magnitude diagrams were generated for each of the $6'.6 \times 6'.6$ fields.

¹Visiting Astronomer, European Southern Observatory.

A total of 13 non resolved objects with a significant color excess were detected as QSO candidates at a redshift similar to that of the target. All the candidates are significantly fainter than the reference QSOs, with only 2 of them within 2 magnitudes of the central object. Follow-up spectroscopic observations have shown that 5, i.e., about 40% of the candidates, are QSOs at the same redshift of the target; 4 are QSOs at different z (two of them probably being a lensed pair at $z = 1.47$); 2 candidates are unresolved HII galaxies at $z \sim 0.3$; one unclassified and one candidate turned out to be a CCD flaw. These data indicate that at least 10% of the QSOs at $z \sim 3$ do have companions.

We have also detected a number of resolved, rather bright Ly α Emitter Candidates. Most probably a large fraction of them might be bright galaxies with [OII] emission, at $z \approx 0.3$. The fainter population of our candidates corresponds to the current expectations. Thus, there are no strong indication for the existence of an overdensity of Ly α galaxies brighter than $m \approx 25$ around QSOs at $z \approx 3$.

Subject headings: QSO: companions: high redshift clustering:

1. Introduction

Quasars are among the most energetic objects known, and as such they can be observed at very high redshift. It is therefore tempting to use them as tracers of the properties of the distant Universe. However, their relation to the physics of the far Universe is not yet well established, in particular their link with galaxy formation and early evolution, and with density enhancements. If there exist a measurable relation, then QSOs could be used as light houses to study those phenomena at high redshift.

Whatever the mechanisms to form and feed QSOs are, it seems that they would be associated with dynamical activity, merging in particular (Kauffmann & Haehnelt (2000)), perhaps in regions of higher than average density where the merging processes would be more frequent. It is well known that at low redshift ($z \leq 0.6$) QSOs are not frequently found in pairs, and very seldom sitting in clusters or dense groups (Komberg & Lukash (1994); del Olmo & Moles (1991)). However, the situation might be different at high- z , when massive galaxies are forming and merging processes are frequent. Indeed, QSOs could be associated with massive primordial galaxies, or be the result of violent interaction among galaxies (merging or galactic cannibalism) which would be more frequent in the central parts of massive clusters (Komberg & Lukash (1994)). If this is the case, high redshift QSOs would tend to appear associated in pairs or small groups, probably located in overdense regions.

There are a number of arguments which support those views. Regarding the spatial QSO distribution, it is known that the QSO 2-point correlation length is similar to that of normal galaxies, $r_o \approx 5-6h^{-1}$ Mpc (Croom *et al.* (2001)), at all redshifts (La Franca, Andreani, & Cristiani (1998); Croom *et al.* (2001)). Moreover, the distribution of pairs of QSOs (with projected angular distance $\theta < 10^\circ$) is similar to that of galaxy cluster pairs (Komberg & Lukash (1994)). Results by different teams do support the idea of some QSO grouping at high redshift. Stephens *et al.* (1997) found three close quasar pairs at $z > 2.7$ based on the Palomar Transit Grism Survey. Campos *et al.* (1999), have identified a number of Ly α Emission Candidates (LECs) in a field that shows a decrement in the CMBR temperature, supposedly produced by an unseen cluster at $z \approx 2.5$. Three of the identified objects in the field (of which 2 were previously known) are QSOs at the same redshift. It can also be mentioned the result by Pentericci *et al.* (2000), who have found a number of LECs around a powerful radio galaxy. One of the objects that has been confirmed spectroscopically is a QSO at a redshift slightly higher than that of the radio-galaxy itself. The last empirical argument is related to the density peak found by Steidel *et al.* (2000) at $z \approx 3$. It also contains a QSO in one of its sub-condensations.

It has been shown by Tyson (1986) that the environments of bright QSOs at intermediate z values show an enhanced projected galaxy density compared to the general field. Clustering at redshift ≥ 2 is still poorly constrained by observational data. However, evidence for clustering is going to grow rapidly with the advent of Large Telescopes. Steidel *et al.* (2000) have recently presented strong evidence of a significant concentration of galaxies at $z \approx 3$ based on Lyman-break color selection. Fynbo, Möller, & Thomsen (2001) and Möller & Fynbo (2001) have measured star formation rates on seven Ly α emitting galaxies located in a filament at $z \approx 3$, detected with narrow-band imaging techniques, and confirmed spectroscopically.

Direct searches have not yet given definitive answers (Keel *et al.* (1999), and references therein). The identification of luminous objects associated with forming clusters would be of great help in the study of matter at high redshift. If the nature of QSOs or, in general, very energetic objects, is somehow related to the density of their environment (at least in the early epochs of galaxy formation), then would we expect small scale clustering of QSOs, and clusters around every QSO? A question that is difficult to unambiguously answer by means of previous QSOs catalogs, as they are based on surveys that search for the presence of radio emission, UV excess or strong emission lines. Here we address this question directly.

In this work we present the results of a photometric search for LECs around 47 QSOs at $z \sim 3$. We also report the spectroscopic follow up of 12 of the 13 unresolved candidates we found. The observational strategy used to look for candidates is discussed in Section 2. The

results are presented and discussed in Section 3. In order to consider QSOs separately, we pay special attention in classifying stellar and non-stellar candidates. The discussion and summary are given in Section 4.

2. Observations and data reduction

In order to study the clustering properties of high redshift QSOs at small scales, and their possible association with galaxy clusters, we carried out a systematic search for strong Ly α emitters in the neighborhood of known QSOs. Based on the VLT filter availability (see Table 1), we selected all known QSOs in the southern hemisphere, with redshift within the ranges $2.863 \leq z \leq 2.959$, and $3.090 \leq z \leq 3.222$. Our initial target list included 27 and 36 objects respectively, with RA between 21h and 5h.

2.1. Observational Strategy

The combination of a narrow band filter (n) at the wavelength of redshifted Ly α , and a wide filter (w) to measure the continuum has been used by numerous authors to detect LECs (see Steidel *et al.* (2000), and references therein). By defining the zero point of the $(w - n)$ color index as that corresponding to pure continuum objects, any significant, positive color excess serves to identify LECs. That zero point is dependent on both the filters and the colors of the pure continuum objects.

To calculate the optimal filter combinations, take $f(\lambda)$ as the flux distribution of a given object, and $S_w(\lambda)$ and $S_n(\lambda)$ the filter transmission functions in the wide and narrow filters respectively. The $(w - n)$ color index is given by

$$w - n = -2.5 \log \left(\frac{\int f(\lambda) S_w(\lambda) d\lambda}{\int S_w(\lambda) d\lambda} \right) + 2.5 \log \left(\frac{\int f(\lambda) S_n(\lambda) d\lambda}{\int S_n(\lambda) d\lambda} \right)$$

For a pure, flat continuum object, $(w - n)$ is obviously zero. For some fixed, non-flat continuum, the value of $(w - n)$ will be at its minimum when both filters are centered at the same wavelength. Therefore, to minimize color effects, we choose filter sets such that the narrow one is always contained in the broad one (see table 1).

With the above definition of $(w - n)$, an object with emission lines in the redshift range surveyed by the narrow filter (approximately given by its FWHM) would have a positive color index. And all the objects with emission lines within the range of the broad filter, but out of the narrow one, would produce a negative color index. In fact, the presence

of absorption lines would produce the opposite effect. However, to produce a significantly positive color index, that absorption in the wide filter should be very strong to compensate for the width of the filter.

To illustrate the expected $(w - n)$ colors, we present in Figure 1 the results of color simulations carried out for one of the filter combinations. Notice that other than the zero-color sequence produced by the pure continuum objects in the field, there is a second quasi-sequence, with a negative color index. This is due to objects with emission lines out of the range of the narrow filter, but within the broad one. The shape of the sequence depends on the shape of the broad band filter. If the filter is a top-hat shaped filter the effect of the emission line is almost independent of its position within the filter, except when near to the edges. Simulations also show how color indices are distributed. It is clear that the precise value of the color index will depend, other than on the redshift and the strength of the line, on its FWHM. When the emission line is broader than the narrow filter, the color index is smaller.

2.2. Contamination and losses

When looking for QSO-candidates, one potential problem is the misidentification of stars as QSOs. Depending on the filters and the spectral type, a star can produce a positive $(w - n)$ color index that could be misclassified as a $z \approx 3$ quasar candidate. In order to estimate the number of misidentifications we have calculated the $(w - n)$ index for different types of stars using two spectral libraries (Gunn & Stryker (1983); Jacoby, Hunter, & Christian (1984)). These libraries include spectral classes from O to M, and luminosity classes from III to V. The results are illustrated in Figure 2, which shows that the stellar colors are well grouped around zero, and that a strict upper limit can be defined.

Another consideration is that some real QSOs may be lost if they don't produce a high enough color index. Indeed, a $\text{Ly}\alpha$ emission QSO can produce a zero or even negative color index depending upon its characteristics and the precise position of the line in the spectral region covered by the filters. In fact, some of our target QSOs do have such color indices. Examination of their spectra shows that in most cases this is due to the presence of a strong absorption in the region of the $\text{Ly}\alpha$ line. It appears that these types of losses can be as high as 50% when the filter combination $F_{485} - \text{HeII}/3000$ is used, whereas it is only 20% for the $g_{\text{Gunn}} - [\text{OIII}]$ combination. For the other filter combinations the losses are negligible.

Although not a serious problem, other emission line objects or QSOs at other redshifts can be confusing when lines other than $\text{Ly}\alpha$ fall in the region covered by the narrow band

filter. For unresolved candidates, a first approximation to the contamination effect can be estimated using the 2QZ catalog². We give in Table 2 the redshift range and the lines that could produce color indices that mimic those of a $z = 3$ QSO. From the same 2QZ catalog we find that the number of QSOs in the other redshift ranges amounts to about 4 per square degree, down to the catalogue limit of $B \sim 21$. Therefore, contamination by bright QSOs should not be a problem, with only 1 or 2 expected in our field of view. Given the magnitude limit of our survey, and assuming an homogeneous distribution of QSOs, a total of at about 8 QSOs at redshifts different from the central one would be expected in our case. As discussed before, some candidates can go undetected depending on different aspects and, therefore, those numbers should be considered as upper limits. All in all, it is unlikely that our list of point-like candidates could be heavily contaminated by stars or by bright QSOs at a different redshift, even if the contamination by fainter QSOs could be sizable.

It is also possible that some unresolved HII galaxies at $z \approx 0.3$ could be falsely identified as QSO candidates. This effect cannot be properly estimated since very little is known about the distribution of compact HII galaxies. The situation is different for resolved candidates, since the effect of the [OII] line of faint HII galaxies at $z \approx 0.3$ could be mistaken as due to LECs. We will discuss further this aspect below.

2.3. Imaging

Observations were performed with FORS1 at ANTU VLT on the nights of 22 and 23 October, 2000. Observing conditions were clear and photometric with seeing between $0''.4$ and $1''.0$. The CCD camera at FORS1 has a pixel size of $0''.2/\text{pix}$, giving a total field of view of $6'.6 \times 6'.6$. For each QSO we acquired images with a narrow band filter covering the wavelength of the redshifted $\text{Ly}\alpha$ line, as well as a broader band filter to get the $(w - n)$ color index. We exposed 3×20 seconds with the broad band filters (*special 485* (F_{485}) and g-Gunn respectively) and 3×200 seconds with the narrow band filters (HeII 472.6, HeII 478.1, [OIII] 500.1, [OIII] 504.5, [OIII] 510.5). Landolt standard stars were observed at various air masses to calibrate the data. Extinction terms and their uncertainties are presented in Table 1. In 2 nights at the VLT we observed 47 fields, i.e. a number of objects large enough to allow a meaningful statistical analysis.

Image detection, photometry and classification were performed using the Source Extractor (SExtractor) software program (Bertin 1996). Image analysis proceeded as follows: CCD

²The 2dF QSO Redshift Survey (2QZ) was compiled by the 2QZ survey team from observations made with the 2-degree Field on the Anglo-Australian Telescope.

images were sectioned in sub-areas of 64×64 pixels. A background map was constructed. The local background histogram was clipped iteratively until convergence at 3σ was reached. These raw background values were then filtered using a median filter (in 3×3 sub-areas), and a bi-cubic-spline was used to obtain the resulting background map. The background map was then subtracted from the image. All objects with a threshold $\geq 1.5\sigma$ above the sky level, and with a minimum area of 5 pix^2 were selected and extracted. Their total magnitudes were calculated by integrating the intensity within elliptical apertures. Finally, the star/galaxy classification (non-resolved/resolved objects) was done with a neural network routine developed by Bertin (1996). This is a training program that classifies objects with an index (stellarity index) between 0 (galaxies), and 1 (stars). It uses eight isophotal areas, the peak intensity, and the seeing information to classify the objects. All the objects that SExtractor had no problem with their photometry (i.e. SExtractor’s `FLAG` = 0) were selected.

The zero point of the broad band magnitudes was set to 27, which results in QSOs magnitudes close to their catalog V magnitudes. The color index zero point was set after examining the resulting color-magnitude diagrams, as corresponding to the sequence seen in the simulations. The threshold to accept the color index of a non resolved candidate as positive was established after considering two effects. First, we took into account the width of the band defined by the stellar colors. They are different for the different filter combinations: 0.15 mag for the F485-HeII/3000 set, 0.10 for F485-HeII/6500, Gunn g-[OIII]/50 and Gunn g-[OIII]/3000 sets; and 0.05 for the Gunn g-[OIII]/6000 set. Second are the observational errors. There are well defined trends of errors with the broad-band magnitude, with 1σ errors of 0.18 mag at $w = 23.5$. We decide however to use the error of each individual object. The reason is that, for a given flux in the broad filter, the LECs will have in the narrow filter a higher signal than the non emitting objects. Thus, adopting instead the average error trend would penalize the detection of LECs. Unresolved objects were finally flagged as LECs when their color index exceeded the sum of the corresponding width of the stellar sequence, and 3.5 times the error of their $(w - n)$ index.

Resolved objects were considered as candidates when their color indices exceeded than 5 times the error in their measured color.

2.4. Spectroscopy

Long slit observations of 12 QSO candidates were carried out on 3 nights in September 2002, using LDSS2 on the Baade telescope at the Las Campanas Observatory. The slit width was $1''$ and the CCD pixel size was $0.380 \mu\text{m}$. The slit was aligned along the line connecting either two member candidates or a candidate and the central QSO. Exposure times ranged

from 1800 to 3600 seconds. The data were taken in non photometric weather and the seeing varied from $0''.6$ to $1''.4$.

The spectra were reduced with IRAF. The data were first bias subtracted and flat-fielded. Sky removal was done by subtraction of sections adjacent to the spectrum in the slit. Wavelength solutions were calculated from Helium-Argon arc lamp exposures. The rms fit of the arc lines given by IRAF is $0.5\text{\AA}/\text{pixel}^{-1}$ while using a 4th order polynomial to fit approximately 25 lines. The wavelength coverage is approximately 3700\AA to 7500\AA with a linear reciprocal dispersion of $5.3\text{\AA}/\text{pixel}$. Cosmic rays were removed via the COSMICRAY routine.

3. Results

3.1. Imaging

Figure 3 shows the color index $(w - n)$ versus the broad-band magnitude, w , and Figure 4 gives the detection threshold, $((w - n) - 3.5\sigma)$, versus w . We have plotted together all the fields observed with the same filter combination. As discussed in the previous sections, $(w - n)$ is positive for objects with some emission line lying within the narrow band filter, and negative when an emission line falls in the broad band filter. From the previous considerations, all objects with $(w - n)$ over the defined threshold are LECs in the redshift range determined by the width of the narrow band filter. The unresolved LECs are QSO candidates at the same redshift of the central QSO. Resolved objects could be galaxies at the central QSO redshift. The images of all the LECs were visually inspected on the processed images. If the object presented distortions, or if it was too close to the edge of the frame, or if a nearby object might be affecting the photometry, then it was eliminated from the list of candidates.

Adopting a flat cosmological model with $H_0 = 70 \text{ km s}^{-1} \text{ Mpc}^{-1}$, $\Omega_m = 0.3$, $\Omega_\Lambda = 0.7$, the size of the field covered by our frames corresponds to $12.2 \times 12.2 \text{ Mpc}^2$, comoving size, *i.e.*, about 1.5 times the clustering scale length of QSOs found by Croom *et al.* (2001). In the radial direction, the redshift range covered by each of our narrow band filters translates into $\sim 50 \text{ Mpc}$.

3.1.1. QSO candidates

The main results concerning unresolved LECs, are presented in Tables 3, 4, and 5. We found a total of 13 QSO-like LECs in 11 fields. In two fields (#14 and #43) there are two candidates. As we already argued, this is a lower limit to the number of candidates. It is interesting to note that those companions have broad-band magnitudes significantly fainter than the central QSO. Therefore, if there is some grouping of QSOs at high redshift, the members have significantly different luminosities.

We have also considered the spatial distribution of the QSO-candidates around the central QSO. In Figure 5 we present the cumulative, normalized distribution of the radial distances from the QSO-candidates to the targets for each set of filters. Given the small number of candidates no firm conclusion can be extracted; however, the candidates appear to be closer than would be expected for a random distribution.

Spectra for 12 of the 13 QSO candidates and 5 central QSOs were obtained, although one candidate turned out to be a CCD cosmetic defect. After extraction, wavelength reduction and flux calibration, we proceeded to classify the spectra and measure redshifts. The resulting spectra are presented in Figures 6, 7 and 8 and their classification are listed in Table 8.

As a result, 5 out of 12 candidates show Ly α in the narrow band filter, therefore, these are QSOs at the central QSO redshift. Thus, as argued before, a minimum of 10% of the surveyed $z\sim 3$ QSOs have companions at the same redshift and, therefore, pairing of QSOs at high redshift would be not infrequent.

Four of the other candidates are also QSOs, but at different redshifts. Two in the field of the QSO #14 have very similar spectra and could be a lensed pair. Two unresolved candidates turned out to be faint HII galaxies at $z\sim 0.3$. The last candidate spectrum has too low signal to noise ratio for a proper classification.

3.1.2. Resolved candidates

Although our main interest was the clustering of QSOs, we have also found a number of resolved LECs. Tables 6 and 7 list the main results determined from the 96 resolved LECs in 34 fields. These data shows that the number of candidates brighter than $m = 23.5$ is much higher than expected from the measured Luminosity Function (LF) of Ly α Break Galaxies (LBG) at $z\approx 3$ (Adelberger & Steidel (2000)). This excess become even more significant when one takes into account that the number of LECs found represent only a small fraction

(20%) of the LBGs that would also be Ly α emitters.

The most plausible explanation is that most, or even all, of those objects are galaxies at $z \approx 0.3$, with the [OII] line falling in the narrow band window. Many of these objects are in fact just barely resolved, probably corresponding to HII galaxies which have a characteristic faint continuum with prominent emission lines (see Terlevich et al. (1991)). The [OII] line is narrow and intense in those objects. Essentially all the objects with an [OII] EW over 60 Å, the median value for the galaxies in Terlevich et al. (1991), would be detected as candidates.

Moreover, four of the bright LECs are found grouped in a field, at the position of a known radio galaxy (NVSS-J104545-012252), with which they could define a cluster at redshift ≈ 0.3 .

In the range $23.5 \leq m \leq 25$, the expected number of Ly α emitters is close to what we have found. Therefore it doesn't seem that there is a significant overdensity of Ly α emitters around QSOs, in that magnitude range. Fynbo et al (2001) have suggested that there may be an excess of fainter Ly α emitters around some QSOs, however, we cannot address this issue given the magnitude limit of our survey.

Figure 5 shows the radial distribution of all the resolved candidates. This distribution is not far from what would be expected for a random distribution. When only the faint candidates are taken into account, the result is even closer to the expectation for a random distribution.

4. Discussion and Summary

We have explored the use of narrow band filters together with broad band filters to detect Ly α emitters around 47 known QSOs.

For unresolved candidates we studied possible contamination from stars by simulating $(w - n)$ colors from stellar spectral libraries covering a wide range of spectral types and luminosities. Contamination by objects with emission lines at redshifts $\neq 3$ was also analyzed.

As a result of the survey we found a total of 13 unresolved LECS in 11 fields. The possible companions to the targeted $z \approx 3$ QSOs are systematically fainter, with only 2 objects within 2 magnitudes of the central QSO. The selection criterion make it very unlikely the these objects are stellar contaminants. Moreover, from the 2QZ catalog we find that contamination by brighter than $B = 21$ mag QSOs at a different z , but with strong lines entering the narrow filter, is very small; none of our candidates are brighter than this limit.

In principle, our candidates could be unresolved Ly-break galaxies (LBG) instead of true QSOs. Before looking at the spectroscopic data, some arguments can be given:

(i) Given the *angular size - redshift* relation, for the geometry we use in this paper, the scale at $z = 3$ is $7.7 \text{ kpc}/''$. Thus $0''.4 - 0''.8$ corresponds to linear sizes in the range between 3 and 6 kpc. At these scales, only very small or extremely nucleated galaxies would appear as unresolved.

(ii) At $z \approx 3$ and $V < 24$, the number of galaxies is very small. As a rough estimate we use the Adelberger & Steidel (2000) luminosity function to calculate the number of Ly-break galaxies at $z = 3$. Assuming that 20% are emission line galaxies, given our geometry and a $50 \text{ Mpc} \times 12.2 \text{ Mpc} \times 12.2 \text{ Mpc} \times 47 \text{ fields} \simeq 3.5 \times 10^5 \text{ Mpc}^3$ volume, we expect 0.0002 ($R < 22.5$), 1.4 ($R < 23.5$), 5.1 ($R < 24$) and 18.5 ($R < 24.5$) Ly-break emission galaxies. However, we find 7, 11, 12 and 13 unresolved objects respectively. Our photometric bandpass is different, but this should not significantly affect these calculations. Therefore our results show a clear excess of unresolved bright objects.

The spectroscopic data confirm that 9 of our 12 candidates are QSOs, 5 of them at the redshift of the target QSO, at $z \sim 3$. From the 2QZ catalog we find that only a very tiny fraction of QSOs have a companion in a volume similar to that of our survey. Due to the lack of data it is hard to extend the analysis to fainter magnitude limits. Nevertheless, starting from the luminosity function of faint AGNs given by Pei (1995, see their Fig. 8), it is possible to deduce that in the range $2.2 < z < 3.3$, there are $\sim 30 \text{ objects deg}^{-2} \text{ mag}^{-1}$ at $B \sim 22.5$, and $\sim 10 \text{ objects deg}^{-2} \text{ mag}^{-1}$ at $B \sim 21.0$. The redshift range covered in our survey is 0.05, which is $\sim 1/22$ of Pei's range. For the area covered by our survey, the expectations would then be $N_{\text{expected}}(B \sim 21) \approx 0.22$ and $N_{\text{expected}}(B \sim 22.5) \approx 0.72$, and we find 0 and 3 respectively. By extrapolating Pei's curve and integrating between 22 and 24, we would expect 2.75 QSOs, and we have found 5. Taking into account the preceding numbers and the possibility to have lost other candidates, as previously discussed, we can conclude that our findings indicate an excess of QSOs around QSOs at $z \sim 3$.

The spectroscopic results confirm the reliability of our photometric technique to detect QSO companions. Nearly half of the candidates have been confirmed as QSOs at the same redshift of the central object, and none were found to be stars.

Our search has also produced a number of resolved LECs. We argue that the majority with $m \leq 23.5$ are probably galaxies with [OII] emission at $z \approx 0.3$, many of them being HII galaxies. In particular, 4 of the resolved LECs appear grouped in one field, close to a known radio galaxy (NVSS-J104545-012252), and could be part of a larger group at that redshift.

The density of resolved LECs in the range $23.5 \leq m \leq 25$ is close to the expectations

from the LF given by Adelberger & Steidel (2000) for LBG, provided that about 20% of them are also Ly α emitters, as pointed out by Steidel *et al.* (2000). The radial distribution of detected LECs around the target QSOs is very close what would be expected for a random distribution.

We acknowledge the *Proyecto de Cooperación CONICYT(Chile)/CSIC(España)* for partial financial support. LI thanks *proyecto FONDAP and P. Universidad Católica de Chile* for funding part of this project. J. Varela acknowledges a grant FP98-52349748 from the *Ministerio de Ciencia y Tecnología* of Spain. This research was partially funded by the Spanish *Ministerio de Ciencia y Tecnología*, grant PB98-0139.

This research benefitted from the use of the VizieR catalog access tool and Aladin, CDS, Strasbourg, France. This research has made use of the NASA/IPAC Extragalactic Database (NED) which is operated by the Jet Propulsion Laboratory, California Institute of Technology, under contract with the National Aeronautics and Space Administration.

We would also like to thank P. Hall and E. Pérez for helping us with the quasar identification, and Andrew Stephens and Eric Gawiser for a careful reading of the manuscript.

REFERENCES

- Adelberger, K. L. & Steidel, C. C. 2000, ApJ, 544, 218
- Bertin, E. and Arnouts, S. 1996, A&A
- Campos *et al.* ApJ Lett 511, L1
- Croom, S. M., Shanks, T., Boyle, B. J., Smith, R. J., Miller, L., Loaring, N. S., & Hoyle, F. 2001, MNRAS, 325, 483
- Fynbo, J. U., Möller, P., & Thomsen, B. 2001, A&A, 374, 443
- Gunn, J. E. & Stryker, L. L. 1983, ApJS, 52, 121 1994, MNRAS 269, 277
- Jacoby, G. H., Hunter, D. A., & Christian, C. A. 1984, ApJS, 56, 257
- Kauffmann, G. & Haehnelt, M. 2000, MNRAS, 311, 576.
- Keel, W. C., Cohen, S. H., Windhorst, R. A., & Waddington, I. 1999, AJ, 118, 2547
- Komberg, B. V., & Lukash, V.N.
- Kurk, J. D., Röttgering, H. J. A., Pentericci, L., Miley, G. K., van Breugel, W., Carilli, C. L., Ford, H., Heckman, T., McCarthy, P., & Moorwood, A. 2000, A&A, 358, L1
- La Franca, F., Andreani, P., & Cristiani, S. 1998, ApJ, 497, 529
- Möller, P. & Fynbo, J. U. 2001, A&A, 372, L57

- del Olmo, A. & Moles, M. 1991, *A&A*, 245, 27
- Pei, Y.C. 1995 *ApJ*1995, 438, 623.
- Pentericci, L., Kurk, J. D., Röttgering, H. J. A., Miley, G. K., van Breugel, W., Carilli, C. L., Ford, H., Heckman, T., McCarthy, P., & Moorwood, A. 2000, *A&A* 341, 329
- Rees, M., 1984, *ARAA* 22, 471
- Shanks, A. and Boyle, 1994, *MNRAS* 271, 753
- Stephens, A., Schneider, D.P., Schmidt, M., Gunn, J.E., & Weimberg, D.H. 1997, *AJ*511, 114, 41
- Steidel, C. C., Adelberger, K. L., Shapley, A. E., Pettini, M., Dickinson, M., & Giavalisco, M. 2000, *ApJ*, 532, 170
- Terlevich, R., Melnick, J., Masegosa, J., Moles, M., & Copetti, M. V. F. 1991, *A&AS*, 91, 285.
- Tyson, A. 1986, *AJ* 92, 691

Table 1. Filters and Extinction Coefficients.

Filter	λ_0 [\AA]	FWHM [\AA]	k
<i>g</i> _{Gunn}	5060	795	0.137 ± 0.016
<i>F</i> ₄₈₅	4850	370	0.176 ± 0.014
<i>HeII</i> /3000	4726	58	0.219 ± 0.028
<i>HeII</i> /6500	4781	68	0.211 ± 0.022
[<i>OIII</i>]	5001	57	0.187 ± 0.030
[<i>OIII</i>]/3000	5045	59	0.186 ± 0.036
[<i>OIII</i>]/6000	5105	61	0.164 ± 0.020

Table 2. Lines that could fall into the narrow band filters for redshifts lower than 3.

Line	Ranges of redshift
$[OIII]\lambda 4959\text{\AA}$	0 – 0.042
$H\beta\lambda 4861\text{\AA}$	0.017 – 0.062
$H\gamma\lambda 4340\text{\AA}$	0.076 – 0.117; 0.139 – 0.190
$[OII]\lambda 3728\text{\AA}$	0.252 – 0.301; 0.326 – 0.386
$MgII\lambda 2803\text{\AA}$	0.665 – 0.730; 0.764 – 0.843
$CIII]\lambda 1909\text{\AA}$	1.445 – 1.540; 1.590 – 1.706
$CIV\lambda 1549\text{\AA}$	2.013 – 2.130; 2.192 – 2.335

Table 3. Unresolved companions

<i>FilterSet</i>	<i>#field</i>	<i>w</i>	<i>w - w_{QSO}</i>	<i>w - n</i>	<i>r_{QSO} (arcsec)</i>
<i>F₄₈₅ - HeII/3000</i>	04	21.95	0.97	0.33	219.0
	14	22.45	3.89	0.31	180.7
	14	22.99	4.43	0.57	182.5
	18	21.69	1.97	0.55	185.6
	25	22.18	3.05	0.45	181.7
<i>F₄₈₅ - HeII/6500</i>	10	23.54	3.50	0.98	118.5
<i>gGunn - [OIII]</i>	52	21.73	4.79	0.39	164.6
	63	22.69	3.07	1.09	85.7
<i>gGunn - [OIII]/3000</i>	30	24.04	3.56	0.72	90.2
	43	21.47	3.92	1.06	152.9
	43	23.17	5.62	0.73	50.0
	44	21.73	2.97	0.20	218.4
<i>gGunn - [OIII]/6000</i>	49	23.53	5.03	0.88	253.8

Table 4. Statistics by number of unresolved companions

Filter Set	$N(w < 21.5)$	$N(w < 22.5)$	$N(w < 23.5)$	$N(w < 24.5)$	$N(Total)$	$\frac{N}{N_{fields}}$	$\frac{N}{d\Omega/dz}$ (#/ \square')
$F_{485} - HeII/3000$	0 0.0 %	4 80.0 %	5 100.0 %	5 100.0 %	5 100.0 %	0.31	0.15
$F_{485} - HeII/6500$	0 0.0 %	0 0.0 %	0 0.0 %	1 100.0 %	1 100.0 %	0.25	0.10
$g_{Gunn} - [OIII]$	0 0.0 %	1 50.0 %	2 100.0 %	2 100.0 %	2 100.0 %	0.13	0.07
$g_{Gunn} - [OIII]/3000$	1 25.0 %	2 50.0 %	3 75.0 %	4 100.0 %	4 100.0 %	0.40	0.19
$g_{Gunn} - [OIII]/6000$	0 0.0 %	0 0.0 %	0 0.0 %	1 100.0 %	1 100.0 %	0.50	0.23
<i>Total</i>	1 7.7 %	7 53.8 %	10 76.9 %	13 100.0 %	13 100.0 %		

Table 5. Statistics by fields with unresolved companions

Filter Set	Number of fields with companions with ...					Number of fields
	$w < 21.5$	$w < 22.5$	$w < 23.5$	$w < 24.5$	any w	
$F_{485} - HeII/3000$	0 0.0 %	4 25.0 %	4 25.0 %	4 25.0 %	4 25.0 %	16
$F_{485} - HeII/6500$	0 0.0 %	0 0.0 %	0 0.0 %	1 25.0 %	1 25.0 %	4
$gGunn - [OIII]$	0 0.0 %	1 6.7 %	2 13.3 %	2 13.3 %	2 13.3 %	15
$gGunn - [OIII]/3000$	1 10.0 %	2 20.0 %	2 20.0 %	3 30.0 %	3 30.0 %	10
$gGunn - [OIII]/6000$	0 0.0 %	0 0.0 %	0 0.0 %	1 50.0 %	1 50.0 %	2
<i>Total</i>	1 2.1 %	7 14.9 %	8 17.0 %	11 23.4 %	11 23.4 %	47 100 %

Table 6. Statistics by number of resolved companions

Filter Set	$N(w < 21.5)$	$N(w < 22.5)$	$N(w < 23.5)$	$N(w < 24.5)$	$N(Total)$	$\frac{N}{N_{fields}}$	$\frac{N}{d\Omega/dz}$ (#/ \square')
$F_{485} - HeII/3000$	4 11.4 %	9 25.7 %	17 48.6 %	24 68.6 %	35 100.0 %	2.19	1.05
$F_{485} - HeII/6500$	0 0.0 %	3 25.0 %	5 41.7 %	6 50.0 %	12 100.0 %	3.00	1.23
$g_{Gunn} - [OIII]$	3 16.7 %	7 38.9 %	12 66.7 %	15 83.3 %	18 100.0 %	1.20	0.59
$g_{Gunn} - [OIII]/3000$	4 16.7 %	14 58.3 %	18 75.0 %	21 87.5 %	24 100.0 %	2.40	1.14
$g_{Gunn} - [OIII]/6000$	2 28.6 %	2 28.6 %	4 57.1 %	5 71.4 %	7 100.0 %	3.50	1.60
<i>Total</i>	13 13.5 %	35 36.5 %	56 58.3 %	71 74.0 %	96 100.0 %		

Table 7. Statistics by fields with resolved companions

Filter Set	Number of fields with companions with ...					Number of fields
	$w < 21.5$	$w < 22.5$	$w < 23.5$	$w < 24.5$	any w	
$F_{485} - HeII/3000$	3 18.8 %	4 25.0 %	8 50.0 %	10 62.5 %	10 62.5 %	16
$F_{485} - HeII/6500$	0 0.0 %	3 75.0 %	3 75.0 %	3 75.0 %	4 100.0 %	4
$g_{Gunn} - [OIII]$	3 20.0 %	6 40.0 %	9 60.0 %	9 60.0 %	10 66.7 %	15
$g_{Gunn} - [OIII]/3000$	4 40.0 %	8 80.0 %	8 80.0 %	8 80.0 %	8 80.0 %	10
$g_{Gunn} - [OIII]/6000$	1 50.0 %	1 50.0 %	2 100.0 %	2 100.0 %	2 100.0 %	2
<i>Total</i>	11 23.4 %	22 46.8 %	30 63.8 %	32 68.1 %	34 72.3 %	47 100 %

Table 8. QSO Candidates Classification

Candidate	<i>R.A.</i> (2000)	<i>Dec.</i> (2000)	<i>z</i>	Lines; class
cnd04	00 47 21.40	-30 14 53.5	2.041	CIV,CIII]
cnd10	01 06 04.56	-37 25 31.7	2.673	Ly α ,CIV,HeII
cnd14-1	01 28 18.11	-35 18 50.5	1.466	CIV,CIII],MgII
cnd14-2	01 28 12.96	-35 20 53.7	1.468	CIV,CIII],MgII
cnd18	03 18 18.39	-20 09 40.6	2.891	Ly α ,CIV,HeII,CIII]; SiIV absorbed by CIV BAL?
cnd25	22 05 49.12	-34 26 04.1	2.801	Ly α , SiII, SiIV+OIV], CIV; BALQSO
cnd30	00 47 15.22	-27 03 40.6	?	
cnd43-1	01 46 01.42	-01 20 43.0	0.351	[OII],[OIII]5007; Starforming galaxy?
cnd43-2	01 45 49.17	-01 21 10.5	3.136	OVI,Ly α ,SiIV,CIV
cnd44	01 46 11.59	-00 43 27.9	3.066	Ly α ,CIV,CIII]
cnd52	04 22 15.98	-38 42 08.3	1.614	CIV(w/absorption),CIII],MgII(weak)
cnd63	23 53 37.22	-01 17 45.5	0.337	[OII],H γ ,H β ,[OIII]; Seyfert 2?

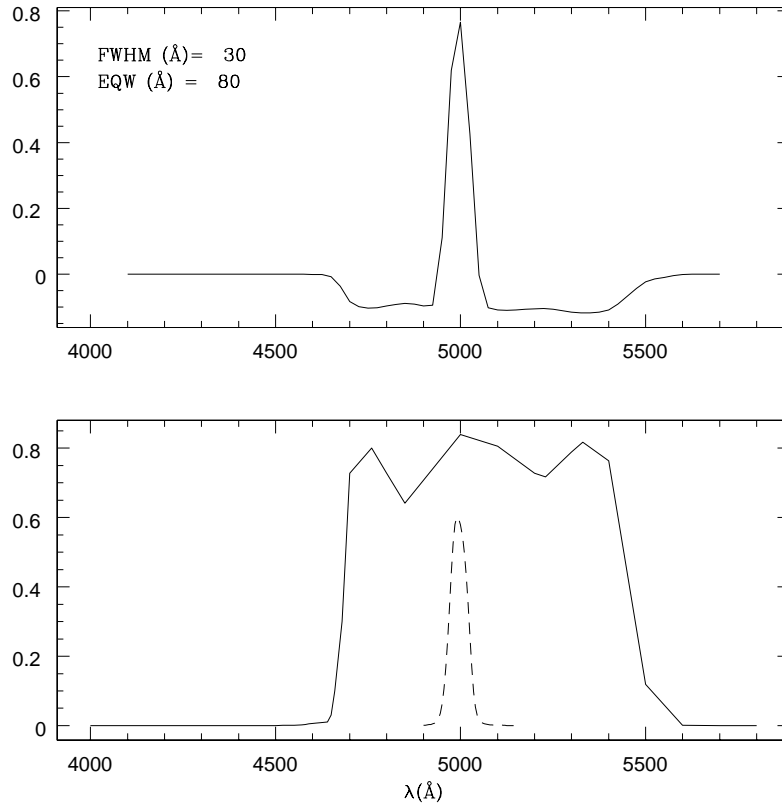


Fig. 1.— The expected signal for an object with Ly α in emission, as a function of the redshift. The curves correspond to the g_{Gunn} and [OIII]500.1 filter combination.

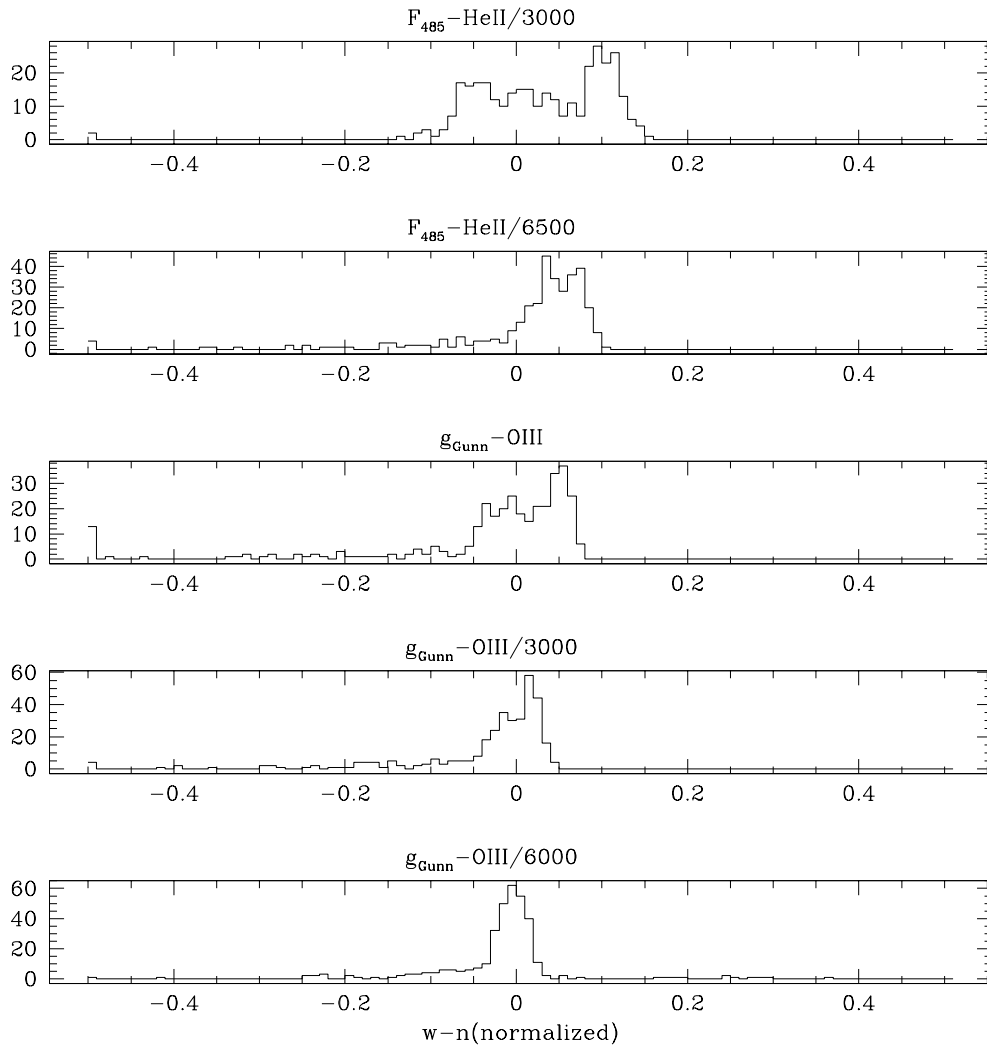


Fig. 2.— Distribution of $w-n$ for a sample of stars for each set of filters

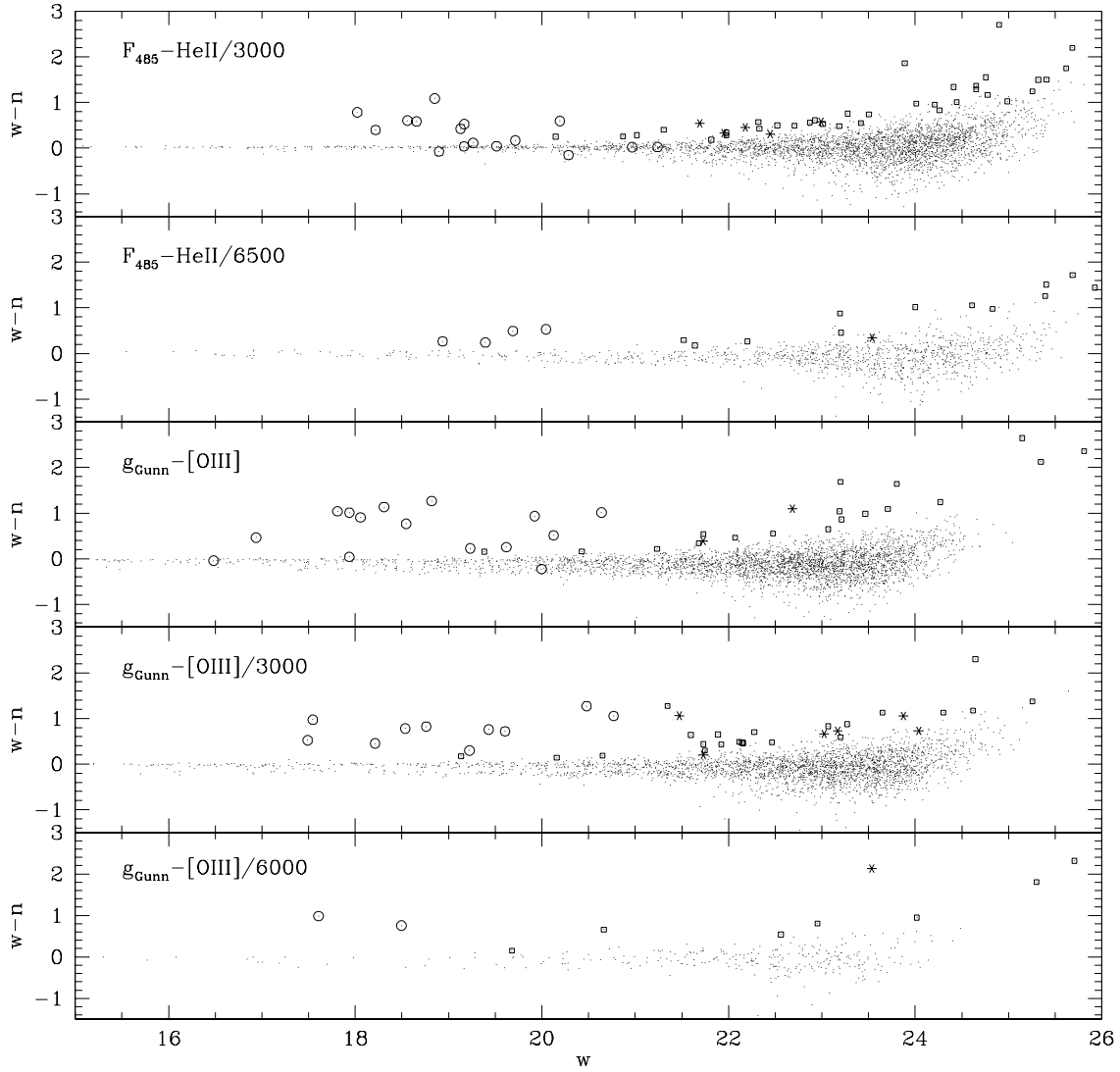


Fig. 3.— Color - magnitude diagram for each set of filters. Circles are central QSOs, stars are unresolved candidates, boxes are resolved candidates, and points are all detected sources.

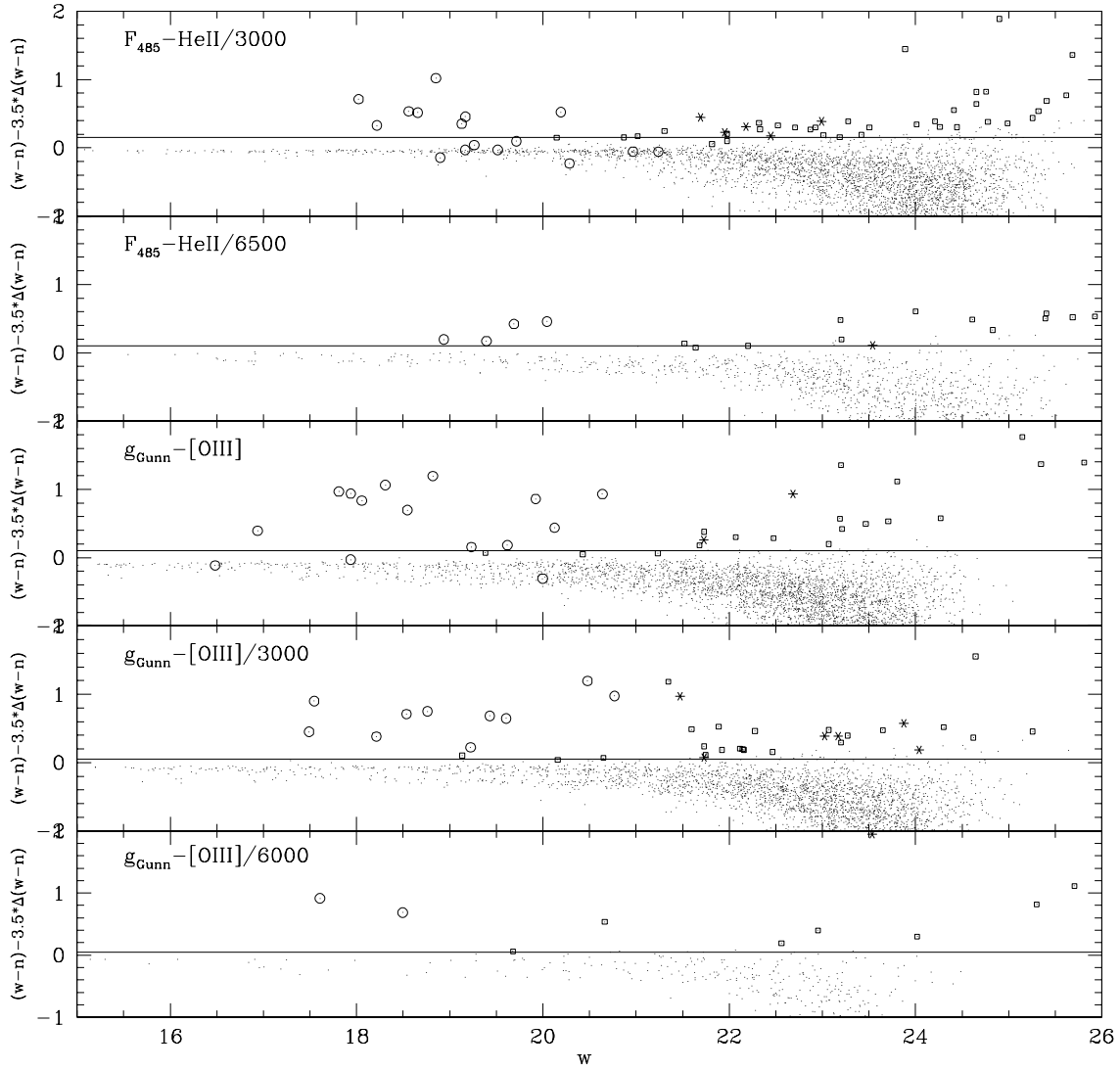


Fig. 4.— Color detection threshold - magnitude diagram for each set of filters. Circles are central QSOs, stars are unresolved candidates, boxes are resolved candidates, and points are all detected sources.

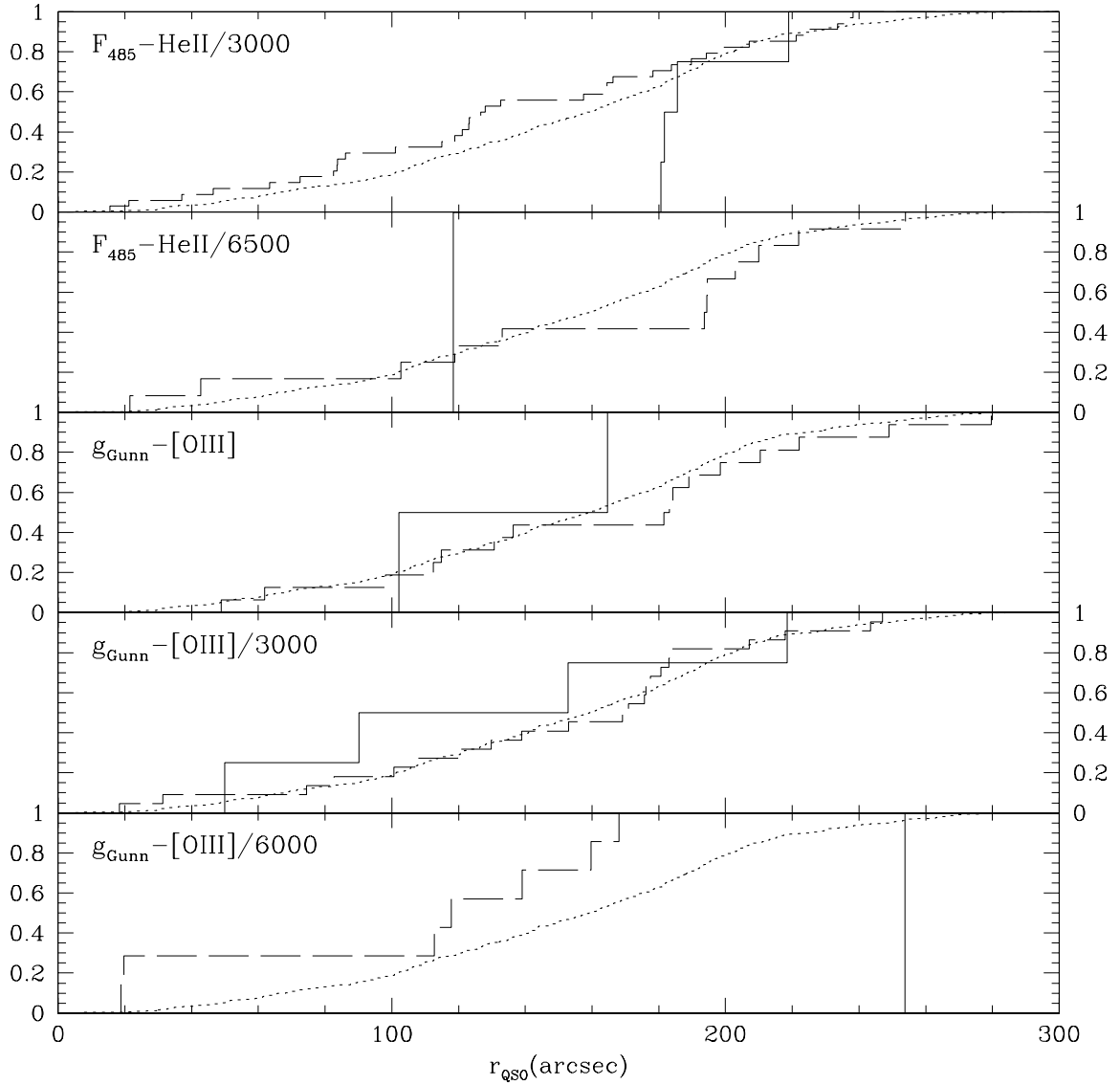


Fig. 5.— Radial distribution of LECs for each filter combination. Solid lines are for unresolved objects, and dashed lines are for resolved objects. The dotted lines illustrate what would be expected for randomly distributed objects.

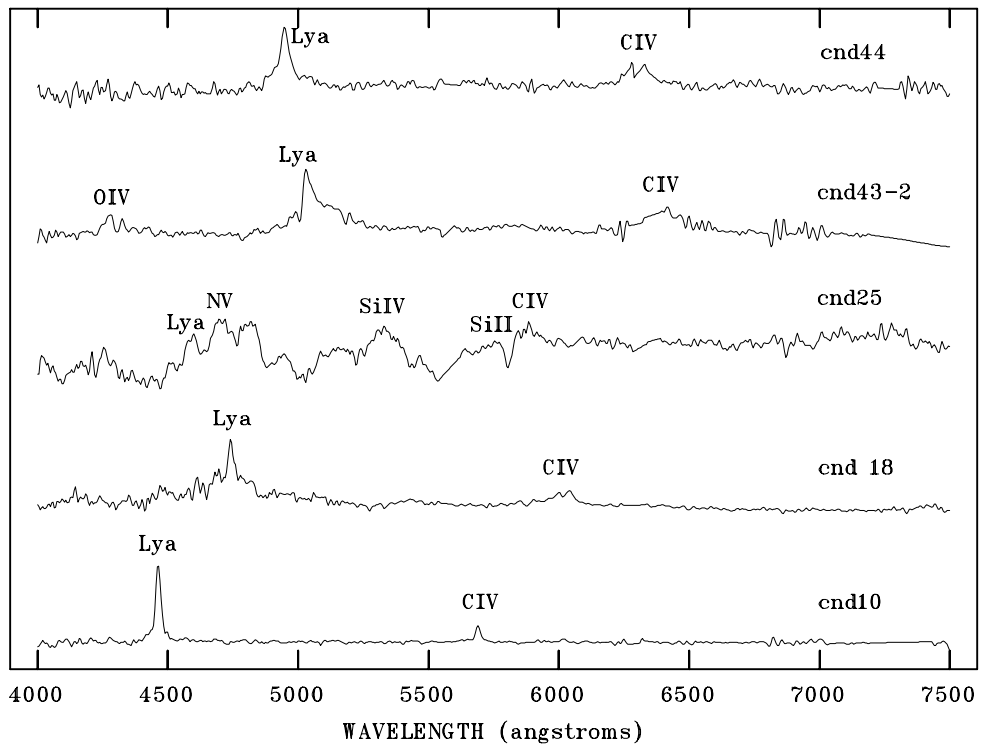


Fig. 6.— Confirmed $z \approx 3$ QSO candidates at the host QSO redshift. The main QSO emission lines are identified.

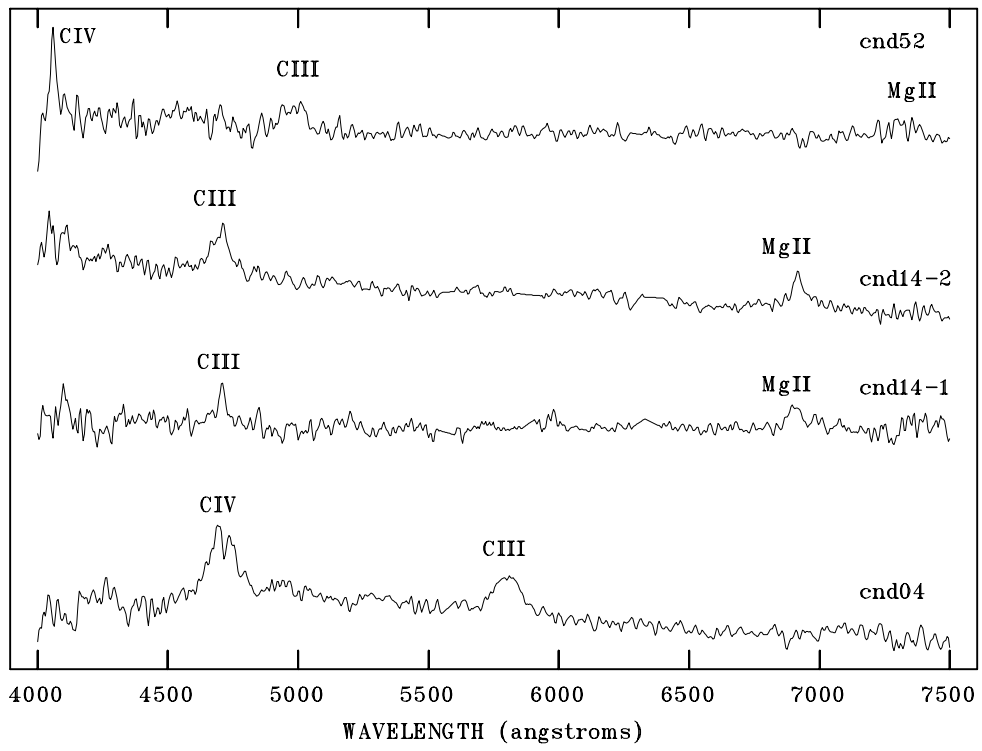


Fig. 7.— QSOs or AGNs not at the host QSO redshift. The main emission lines are identified.

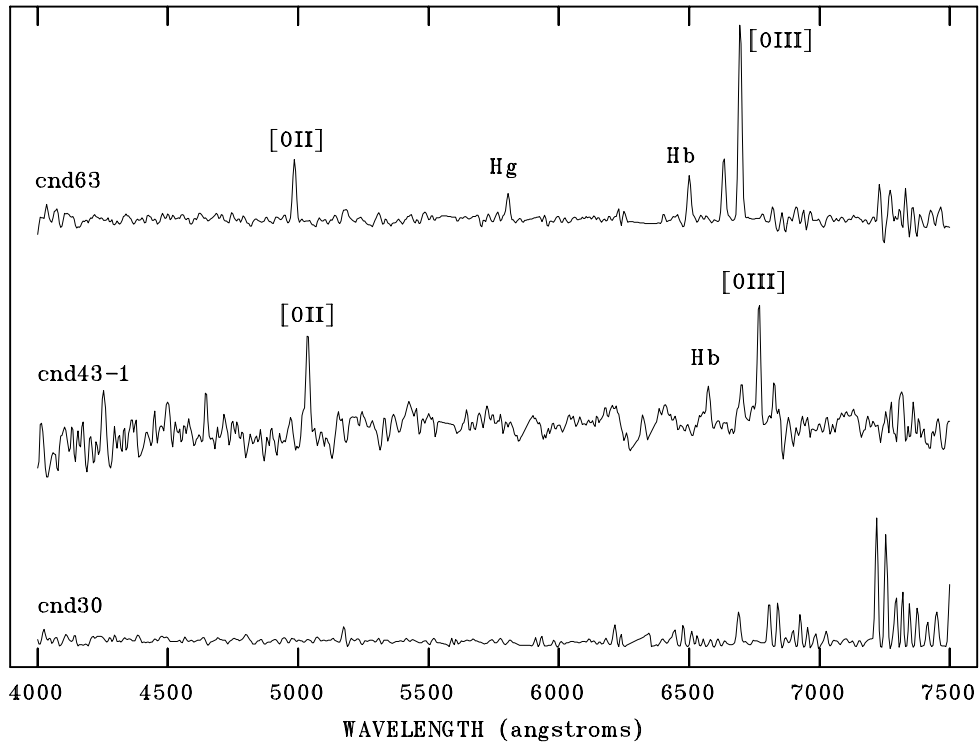


Fig. 8.— Non QSO objects. Most probably, the two top spectra correspond to starburst galaxies. The bottom spectrum has not been identified. The main emission lines are identified.